Journal of Biomolecular NMR, **11:** 319–328, 1998.
KLUWER/ESCOM

Full ^{1}H NMR assignment of a 24-nucleotide RNA hairpin: Application of the ^{1}H 3D-NOE/2QC experiment

Irene M.A. Nooren[a], Ke-Yu Wang[b], Philip N. Borer & István Pelczer[c,*]
Chemistry Department, Syracuse University, Syracuse, NY 13244-4100, U.S.A.

Received 3 October 1997; Accepted 6 November 1997

Key words: homonuclear, multiple-quantum, NMR assignment, RNA, three-dimensional

Abstract

The subject RNA models the binding site for the coat protein of the R17 virus, as well as the ribosome recognition sequence for the R17 replicase gene. With an RNA of this size, overlaps among the sugar protons complicate assignments of the ^{1}H NMR spectrum. The cross peaks that overlap significantly in 2D-NOE spectra can frequently be resolved by introducing a third, in our approach the double-quantum, frequency axis. In particular the planes in a 3D-NOE/2QC spectrum perpendicular to the 2Q axis are extremely useful, showing a highly informative repeating NOE-2Q pattern. In this experiment substantial *J*-coupling confers special advantages. This always occurs for geminal pairs (H5′/H5″ for RNA plus H2′/H2″ for DNA), as well as for H5/H6, for H3′/H4′ in sugars with substantial populations of the N-pucker, for H1′/H2′ for S-puckered sugars, and usually for H2′/H3′. For the 24-mer RNA hairpin the additional information from the 3D-NOE/2QC spectrum allowed assignment of *all* of the non-exchangeable protons, eliminating the need for stable-isotope labeling.

Abbreviations: NOE, nuclear Overhauser effect; 2D, two-dimensional; 3D, three-dimensional; NOESY, 2D NOE spectroscopy; HoMQC, homonuclear multiple-quantum coherence; 2Q-COSY, double-quantum correlated spectroscopy; DANTE, delays alternating with nutations for tailored excitation.

Introduction

A 24-mer RNA has been prepared as a model for the coat protein binding site of the R17 virus, as well as the translational initiation site for the replicase gene. This sequence, which contains a bulged adenine and a hairpin of 4 nucleotides (Figure 1), has been carefully studied by Uhlenbeck and co-workers (Lowary and Uhlenbeck, 1987; Romaniuk et al., 1987; Wu and Uhlenbeck, 1987; Gott et al., 1993). An analysis of the NMR data and preliminary model building for G3-C21 demonstrated that the region from the A8 bulge through residue G16 is quite flexible (Borer et al., 1995). The present paper discusses procedures for obtaining the most difficult assignments using a novel 3D-NOE/2QC experiment and corrects some assignment errors, primarily in G1-A4. Further refinement has resulted in clear distinction of the structural properties of the loop and bulge, as well as the nature of the structure at the single-stranded ends of the molecule (Kerwood and Borer, 1996).

The largest hurdle for beginning to determine RNA structures by NMR is stable-isotope labeling. While ^{15}N- and ^{13}C-labeled nucleoside triphosphates are commercially available, preparing a single 1 mM NMR sample is expensive. Preparation of the labeled NTPs from ribosomal extracts is not technically challenging (Batey et al., 1992; Nikonowicz et al., 1992; Michnicka et al., 1993; Batey et al., 1995), but may require specialized equipment and mastery of biosynthetic methods that may be unfamiliar to a spec-

* Author for correspondence.
[a] Present address: Bijvoet Center for Biomolecular Research, Padualaan 8, 3584 CH Utrecht, The Netherlands.
[b] Present address: Gilead Sciences, 353 Lakeside Dr., Foster City, CA 94404, USA.
[c] Present address: Department of Chemistry, Princeton University, Princeton, NJ 08544, USA.

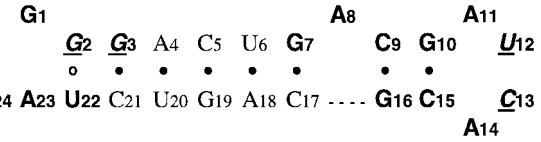

Figure 1. The 24-mer RNA hairpin that binds the R17 viral coat protein. Sugars for residues in normal font are almost exclusively N-puckered; those from G7 to C16, as well as G1 to G3 and U22 to U24, have at least some degree of S-pucker; *G*2, *G*3, *U*12, *C*13, and *U*24 have mixed pucker with 30% or more in S-forms.

troscopist. In addition, heteronuclear isotope labeling with ^{13}C or ^{15}N introduces technical difficulties due to heteronuclear *J* couplings and extra line broadening caused by enhanced relaxation rates. This paper illustrates one of the experimental NMR techniques that circumvent the need for labeling to assign all protons and determine structures of RNA samples with 20–30 nucleotides (Borer and Levy, 1994; Borer et al., 1995, 1997; Kerwood and Borer, 1996), and ^{1}H-^{31}P correlation (I. P., S. Cai, and P. B., unpublished).

About 90% of RNA ^{1}H-signals resonate within ∼0.8 ppm, and the mean spacing of signals is ∼2 Hz/proton in the most crowded part (all comparisons at 500 MHz). These RNA signals in the '*F*-region' (H2′, 3′, 4′, 5′, 5″) are extremely crowded, more so than for DNA and peptides. Typical unapodized linewidths at half-height are ∼6–8 Hz for 20-mer RNA, and all of the *F*-signals are multiplets, so peak footprints at the base of peaks cover 15–40 Hz in this region in unenhanced spectra. This makes the homonuclear approach seem hopeless, but by using two or three carefully selected frequency dimensions and reducing the linewidth of most lines in 2D-NOE spectra by about threefold (Borer and Levy, 1994), full proton assignment can be made. This provides more than a sufficient number of restraints for model building (Kerwood and Borer, 1996). Our 24-mer RNA has MW = 8.5 kDa. We estimate that these procedures should be routinely applicable for assignment and structure determination of DNA with ∼40 residues and proteins with 100–125 residues on 500 MHz spectrometers (Borer et al., 1997).

A number of publications have demonstrated that the addition of further frequency dimensions to NMR spectra relieves many of the difficulties of overlap. Another advantage of multidimensional NMR spectroscopy is that it is feasible to combine features of different 2D experiments. In the ^{1}H homonuclear case, through-bond transfers are restricted to *intra*residual connectivities, while through-space contacts facilitate sequential assignments and determination of the secondary structure. Thus NOESY and COSY (or their spin-locked variants) can be combined in one experiment to carry information both on distances and on *J*-coupling (Griesinger et al., 1989). 3D proton-only experiments combining NOE with TOCSY/HOHAHA have been shown to be extremely useful for making assignments. (Vuister et al., 1988; Oschkinat et al., 1989; 1990; Cieslar et al., 1990; Mooren et al., 1991; Piotto and Gorenstein, 1991; Simorre et al., 1991; Simorre and Marion, 1991; Radhakrishnan et al., 1992). An elegant application of the 3D-TOCSY/NOESY method has been presented for a 12-mer RNA duplex structure (Wijmenga et al., 1994).

In this paper we demonstrate the utility of the 3D-NOE/2QC experiment, a combination of through-bond and through-space magnetization transfer steps in which NOESY (Jeener et al., 1979) and ^{1}H homonuclear 2Q-COSY (Braunschweiler et al., 1983; Mareci and Freeman, 1983) are combined. This experiment can be looked at as a novel extension of 2D methods which combine MQ excitation with another magnetization transfer step, such as homonuclear MQ-RELAY (Macura et al., 1984; Müller and Pardi, 1985), double-quantum NOESY (van de Ven et al., 1985), ZQ-TOCSY (Kessler et al., 1990), and the closely related DREAM sequence (Berthault and Perly, 1989). Homonuclear multiple-quantum filtered NOE and ROE experiments (Kessler et al., 1988) can be also considered as predecessors of the experiment described here.

MQ correlations have several useful properties that confer advantages in making RNA/ DNA assignments: (1) The MQ step is quite efficient for low coupling constant/linewidth ratios (Dalvit et al., 1987), which is especially useful for the H1′-H2′ connectivities in RNA, and for larger molecules with broad lines. (2) MQ correlation peaks show antiphase fine structure by the active coupling; sensitivity can be further enhanced by dispersive phasing of the overlapping antiphase pair (Pelczer et al., 1991b; Bishop et al., 1996). (3) No body-diagonal will be present according to the basic character of MQ correlations (Braunschweiler et al., 1983; Mareci, 1988). (4) 'Remote' correlations, which are unique features of HoMQC spectra (Braunschweiler et al., 1983) introduce characteristic peaks that further enhance the information content of the spectrum. (5) Finally, the MQ transfers do not involve isotropic mixing, and magnetization transfer is limited to one or two steps via *J*-coupled spins. By contrast, procedures that involve TOCSY (HOHAHA) diffuse magnetization rapidly throughout a

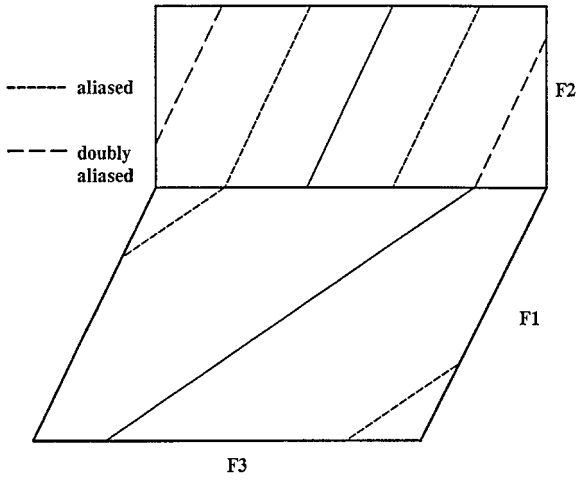

Figure 2. Scheme for aliasing in the indirectly detected dimensions.

sugar ring, resulting in reduced peak intensities compared to MQ correlated spectra. This applies to other *J*-linked systems, as well.

Materials and methods

Sample preparation and experimental conditions

The synthesis, purification, and characterization of the 24-mer has been described (Borer et al., 1995), as well as the refinement of the structure (Kerwood and Borer, 1996). The RNA concentration for the NMR sample was 1.7 mM, and the 0.4 mL sample was dissolved in 0.025 M NaCl, 0.05 M $PO_4{}^{3-}$ adjusted to pH 7.0, 5×10^{-4} M EDTA, 0.01% NaN_3, in 99.96% D_2O. The spectra were acquired at 298 K.

NMR spectroscopy

The 3D NMR experiment was performed on a GN-500 NMR spectrometer at 500.1 MHz.

There are two alternative combinations of the NOE and HoMQC dimensions: either in the order NOE/HoMQC or HoMQC/NOE. The information content of the two experiments is basically the same; however, there are practical aspects which may favor one or the other. Magnetization is antiphase after the read pulse which follows the MQ evolution period. Direct acquisition of this signal will provide the highest spectral resolution, and therefore the least cancellation. Extending the acquisition period to gain resolution has little effect on the overall experimental time. However, radiation damping becomes a serious issue in H_2O solutions at high magnetic fields; then it is better to have the NOE mixing period right before the direct acquisition. During this mixing period the water signal can be brought to the *z* direction by accelerated radiation damping (Jahnke and Kessler, 1994; Sklenár, 1995) and excluded from the acquisition using gradient-assisted purging methods, such as WATERGATE (Piotto et al., 1992). Therefore, NOE/HoMQC has advantages in D_2O and HoMQC/NOE is recommended in H_2O.

Our focus was the nonexchangeable sugar resonances, so we performed the measurement in D_2O, and used the 3D-NOE/2QC pulse sequence, which is shown in Figure 3 together with the phase cycling. A DANTE (Morris and Freeman, 1987) presaturation through the main transmitter was used for suppression of the residual water signal in order to avoid extra noise due to lack of phase coherence between the decoupler and the receiver (Zuiderweg et al., 1986) on our instrument. Using the first sideband of the DANTE, the carrier position was placed close to the base region, allowing a narrower spectral window for the acquisition dimension and reducing the overall size of the time domain data. A short delay was used after the DANTE sequence to allow saturated signals near the water to partially recover. States-Haberkorn-Ruben (SHR; States et al., 1982; Pelczer and Carter, 1997) phase incrementation was used to achieve quadrature detection in F1 and F2. Double-quantum selection was accomplished in four phase-cycling steps (Bax et al., 1980). Removal of single- and multiple-quantum coherences that evolve in the NOE mixing period would require four additional phase cycling steps, while no phase cycling can remove zero-quantum contributions (Neuhaus and Williamson, 1989). In order to save acquisition time, only single-quantum components were suppressed in a two-step phase cycle. Finally, half-CYCLOPS (Stejskal and Schaefer, 1974; Hoult and Richards, 1975; Otting, 1990) phase cycling was applied to remove most quadratic artifacts, resulting in 16 steps per quadratic component (32 per time increment).

A mixing time of 200 ms was used for the NOE transfer and 2×10 ms for the 2Q excitation delay. An extra composite 180° pulse ($90°_{\phi} - 180°_{\phi+90} - 90°_{\phi}$) was inserted in the middle of the NOE mixing time (τ_m) in order to clean the spectrum further (Zuiderweg et al., 1986). The 90° read pulse at the end of the conventional sequence was replaced by a spin-echo sandwich (Rance and Byrd, 1983; Davis, 1989) which allowed optimization of baseline properties along the acquisition dimension. The echo delay

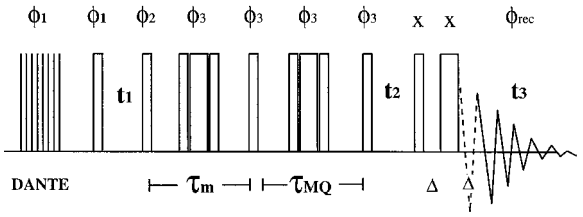

Figure 3. Pulse sequence for the 3D-NOE/2QC experiment. Narrow bars represent 90° rf pulses (except in DANTE, with small flip angle pulses), while wide bars denote 180° rf pulses. The delay after the DANTE is used as a recovery time. The NOE mixing time (τ_m) and MQ excitation delay (τ_{MQ}) are indicated, where the composite 180° rf pulses in the middle of these periods are used as refocusing pulses. The period Δ serves as the echo delay for the read pulse sandwich (see also text). Phase cycling included a two-step procedure for the NOE mixing period and a four-step 2Q filtering cycle for the t_2 dimension for suppression of unwanted coherences: $\phi_1 = \phi_2 = x, -x, y, -y, -x, x, -y, y$; $\phi_3 = x, x, y, y, -x, -x, -y, -y$; $\phi_{rec} = +, -, -, +$, and half-CYCLOPS incrementing all pulses and the receiver by 90°. Sign discrimination in the remote dimensions was accomplished by the SHR method incrementing ϕ_1 by 90°, and, in an independent step, ϕ_1 through ϕ_3 by 45°, respectively, and storing the real and imaginary components separately (see also text).

(Δ) was set nearly equal to two dwell times (Davis, 1989), and fine-tuned to provide an optimally flat baseline (discarding the first two t_3 points prior to FT processing).

The first points were acquired at nearly half dwell time along the indirectly detected dimensions (t_1 and t_2) to avoid necessity for first point correction, ensure a flat baseline, and to introduce useful aliasing properties (Bax et al., 1991; Pelczer and Carter, 1997). The acquisition order was 3-1-2. Phase incrementations were accomplished first in four contiguous blocks, then t_1 was incremented. Time incrementation for t_2 was accomplished in separate acquisitions using the macro capabilities of the GE acquisition software. The final time domain size was $1024^* \times 64^* \times 32^*$ ($t_3 - t_1 - t_2$) points so that the total experiment time was approximately 150 h.

The spectral widths in F1, F2 and F3 were set to 2000 Hz (7.74–3.74 ppm), 1428 Hz (2Q frequencies: 10.62–7.76 ppm) and 3205.12 Hz (9.94–3.53 ppm), respectively. Aliasing along the single-quantum dimension (F1) and the double-quantum dimension (F2) was designed carefully in order to maximize spectral resolution with the least possible overlap. Single aliasing was applied in F1, whereas aliasing two or more times was used in F2 as shown in Figure 2 in order to maximize spectral resolution. The carrier was set between the H6 and H5/H1′ resonances with a few H6 resonances falling just outside the selected spectral window. These resonances aliased from the opposite side in F3. The spectrum was shifted by half of the spectral window in F1 during processing by simple inversion of every other complex point (Pelczer and Carter, 1997) in order to unite the *F*-region and make data analysis more convenient. Homonuclear two-quantum connectivities in RNA show a pattern which can be aliased without risking ambiguities in the assignment or serious overlap (Pelczer and Bishop, 1997).

NMR data processing

All processing was done on Sun and Silicon Graphics workstations, using the *z-ant* format and processing methodology (Pelczer et al., 1992) in NMRZ (New Methods Research, Inc., now Tripos Assoc., Inc., St. Louis, MO). Individual pseudo-2D files were converted to 8 *z-ant*s, which were processed pairwise to combine the files into a 3D all frequency-domain object. Suppression of the residual water signal was performed in the time domain (Marion et al., 1989) after temporary relocation of the carrier position (Bax et al., 1983; Pelczer and Carter, 1997). The 64* points in the t_1 direction were extended to 128* points by linear prediction using the standard protocol available in NMRZ, which uses vector-by-vector processing and the Burg algorithm (see: *NMRZ User Guide*, Tripos Assoc., St. Louis, MO). No distortion of the output data was observed except some occasional spikes and sharp ridges along vectors with no true signal. In the t_3 and t_1 direction a shifted sine bell window function was applied and data were zero-filled once. In the t_2 direction a Gaussian window function was used for apodization and data were zero-filled twice. The resulting fully transformed spectrum (the *RRR z-ant*) consisted of $2048 \times 256 \times 128$ (F3-F1-F2) points (256 MB). It was phased to dispersion-absorption-absorption (*DAA*, F3-F1-F2) mode in order to enhance sensitivity and simplify the structure of cross peaks with partially overlapping antiphase fine structure (Pelczer et al., 1991b; Bishop et al., 1996).

Results and discussion

Analysis of the 3D-NOE/2Q-COSY experiment

The pulse sequence of the homonuclear 3D-NOE/2QC experiment (Figure 3) indicates that chemical shift labeling occurs in t_1, after which magnetization can be transferred through NOE contacts during the mixing period τ_m. Other significant coherence transfers (with

the exception of zero-quantum effects) are largely suppressed by the phase cycling procedure. The read pulse for the NOE segment in the 3D sequence is equivalent to the first pulse in the multiple-quantum excitation sandwich. Subsequently, during a period τ_{MQ}, multiple quantum coherence is generated for the J-coupled spins. Phase cycling removes the single- and other odd-quanta, as well as four-quantum coherences, so that labeling in t_2 takes place by the sum frequency ($\delta_A + \delta_X$) of two J-coupled spins A and X. Finally, coherence is transferred back to the corresponding single quantum frequency, which is detected during t_3.

As a result of the coherence transfer pathway described above, a typical correlation pattern is expected to be similar to that shown in Figure 4a in an F1/F3 plane. The single-quantum frequencies, δ_A and δ_X, are labeled on the F3 axis in the figure. For A and X, this plane is at the double-quantum frequency, F2 $= \delta_A + \delta_X$, with peak intensities affected by $^2J_{\mathrm{AX}}$ or $^3J_{\mathrm{AX}}$ (if J $<\sim$2 Hz, the peaks will be weak or invisible). The diagonal peaks on this F1/F3 'NOE plane' carry information analogous to that of a double-quantum filtered 2D-NOE spectrum (filled circles in Figure 4a) and the open circles represent 'cross-diagonal' peaks. We may call them 'inner' NOEs, because they connect spins which contribute to the MQ coherence. Based on theoretical symmetry of NOE transfer between two spins (Williamson and Neuhaus, 1987), and that for direct correlation peaks in a double-quantum spectrum (Mareci, 1988), the four peaks in this rectangular pattern should have the same intensity. Three-dimensional cross peaks representing NOE connectivity with nuclei outside the group of spins which contribute to the MQ coherence are shown by triangles (Figure 4a). These 'outer' NOEs connect other spins to A or X or both, but not A to X. In contrast to other spectra involving nonselective homonuclear 2D correlations, such as TOCSY and NOESY, there is no equivalent to a body-diagonal. Any remote (or magnetic equivalence) J-correlations involving A or X, e.g., A and I or X and J, will extend to the F2 $= 2Q\{A, I\}$ or F2 $= 2Q\{J, X\}$ planes (Braunschweiler et al., 1983). These repeating patterns are unique features of MQ correlations, and the extensive redundancy makes the homonuclear 3D-NOE/2QC spectrum very useful for assigning systems with a high degree of overlap.

Overlap in the 3D-NOE/2QC spectrum that prevents spectral assignment is rare for 20- to 30-mer RNA. Consider two sets of J-coupled spins, A/X and

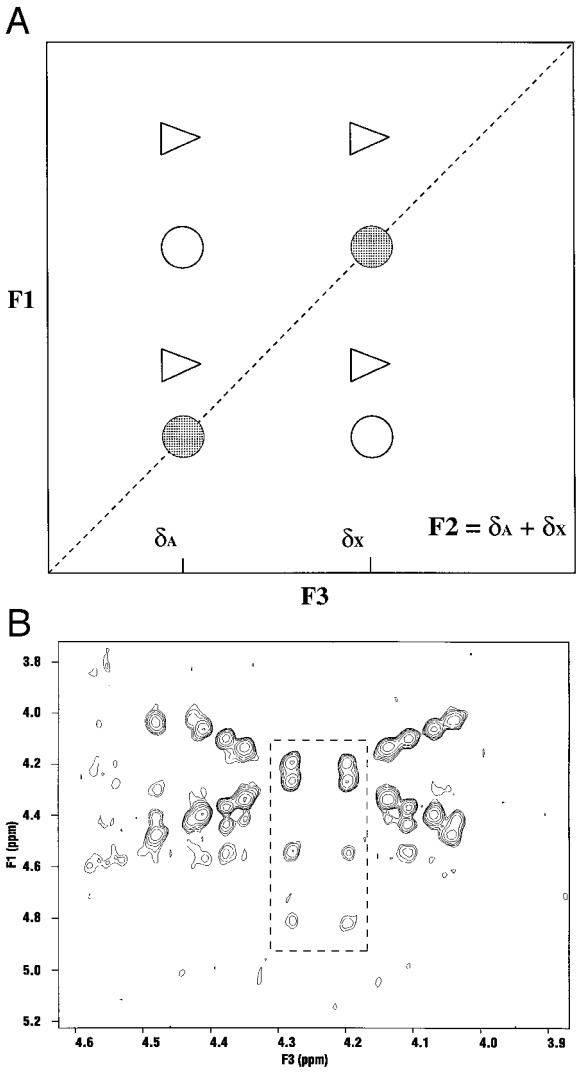

Figure 4. (A) Schematic peak pattern on a NOE plane in a 3D NOE/2QC spectrum. Filled circles denote $2Q_{\mathrm{AX}}$ peaks, while open circles show peaks modulated by $2Q_{\mathrm{AX}}$ and 'inner' NOE. Triangles represent three-dimensional cross peaks, modulated by $2Q_{\mathrm{AX}}$ and 'outer' NOE to a spin other than A or X. Such peaks could be inside or outside of the $2Q_{\mathrm{AX}}$/'inner' NOE pattern. (B) This is illustrated by the F3/F1 NOE plane at F2 = 8.47 ppm. Only positive levels are shown. The dashed frame highlights one of the typical correlation patterns: high intensity, symmetrically arranged 2Q and inner NOE peaks are associated with weaker outer NOE peaks. Several similar patterns can also be identified.

B/Y; the extension to more sets is straightforward. There are three kinds of overlap to discuss. (1) When $\delta_A = \delta_B$, A and B overlap in conventional single-quantum spectra. However, the NOE/2QC patterns for A/X and B/Y will be sorted according to their 2Q frequencies along F2, so the 3D spectrum easily resolves this overlap problem. (2) Overlap of two NOE planes

occurs if $\delta_A + \delta_X = \delta_B + \delta_Y$; then two concentric NOE patterns will be found on the same 2D plane with associated outer NOE contacts (see Figure 4B). (3) Complete overlap of 2Q patterns and 'inner' NOE peaks in the 3D space occurs only if both $\delta_A = \delta_B$ and $\delta_X = \delta_Y$; this is rare even for RNA molecules of the size considered in this paper.

Figure 4b illustrates the second kind of overlap for the F1/F3 plane at F2 = 8.53 ppm of the 24-mer, which is one of the most crowded planes in the 3D spectrum. The diagonal (back-transfer) and cross-diagonal peaks show up as strong peaks while the true three-dimensional cross peaks (outer NOE peaks) are smaller. Some cross-talk to neighboring planes is also present. By contrast, the corresponding region along the diagonal of the conventional 2D-NOE spectrum is hopelessly crowded (Borer et al., 1995). The relatively small degree of overlap, and the lack of a body diagonal makes a 3D NOE/2QC spectrum very useful compared to homonuclear spectra relying on 1Q correlations.

F1/F2 planes are also very useful for connectivity analysis. Such planes are best resolved as they are orthogonal to the high-resolution acquisition dimension and therefore have the least cross-talk with their neighbors (Pelczer and Szalma, 1991). In an F1/F2 plane a pair of strong correlation peaks will be found at locations determined by the F1 1Q frequencies and their mutual 2Q frequency in complete analogy with conventional 2Q-COSY correlations (Mareci, 1988). However, these two peaks are not identical in origin, i.e., one is located on the diagonal in an F1/F3 plane, while the other indicates NOE contact between the *J*-coupled pair. Outer NOE peaks associated with either (or both) of these two spins will show up at the same 2Q frequency. The same pattern will be repeated at the F3 frequency of both *J*-coupled spins. Overlap with other spins is not likely to be the same for both, so the repeated pattern is easy to find in these F1/F2 planes. This feature could also support automation of peak analysis.

Figure 5 presents a real example of segments selected from F1/F2 planes at 2Q frequencies of pyrimidine H5-H6 *J*-coupled pairs (J $\cong$ 8 Hz). The bottom two strips were selected at the F3 frequency corresponding to U24, H5 and H6; only the H5 strips are shown for the other H5/H6 pairs. The two large peaks in the bottom two strips at ~7.5 and ~5.3 ppm correspond to U24,6 and U24,5, respectively. Outer NOEs appear in the strips at ~5.6 ppm (U24,1′), ~4.6 ppm (A23,2′ and 3′;U24,4′), ~4.3 ppm (U24,5′), ~4.2 ppm (U24,3′), and ~4.1 ppm (U24,2′ and 5″). At the mixing times used in this experiment, outer NOEs to i(H5/H6) from i(H1′, H2′, H3′, H4′, H5″) routinely contribute to the intensities, as do those to i(H5/H6) from i−1(H1′, H2′, H3′, H5, H6) within A-family helical regions (N-sugar puckers). The U24,5 strip at F2 = 9.92 ppm (next to bottom) suffers partial overlap with C5,5 (9.84 ppm), C9,5 (9.93 ppm), and U20,5 (9.87 ppm). The primary interference is between the strips selected at the F3 value corresponding to U24,5 and C5,5, which have identical chemical shifts. However, even this interference is resolved in the U24,6 partner strip. This illustrates the general property of the 3D NOE/2QC spectrum that extensive redundancy allows resolution of most overlap problems.

Base, H1′ and H2′ assignments

The base, H1′ and H2′ protons of the 24-mer were securely assigned from 2D NOE and 2D 2QC spectra (Wang, 1991). The known single quantum frequencies of the H6, H5, H1′ and H2′, which are listed in the first four columns of Table 1, were used to predict the 2Q{H6,H5} and 2Q{H1′,H2′} patterns at the corresponding F2 frequency. Note that all of the peaks in Figure 5 are aliased once, except for C15,5, which is aliased once in F2 and once in F1. This improves the resolution in the incremented dimensions. Thus, the F2 frequencies for the strips are: δ(H6) + δ(H5) −2.82 ppm (except for C15,5). The aliasing was applied carefully, to avoid any significant overlap. Only the 2Q{H6,H5} were aliased in F2 and some base resonances in the F1 direction. Similar multiple aliasing has proven useful in the carbon dimension for protein studies (Bax et al., 1991). Peaks that are aliased once have opposite signs from those which are not aliased or those that are aliased twice, because the first t_2 and t_1 points were acquired at half dwell time (Bax et al., 1991). Also, dispersive phase correction in F3 converts the antiphase peaks that result from normal phase correction to primarily positive intensity.

In contrast with the 2Q{H6,H5}, the intensity of 2Q{H1′,H2′} strongly depends on the sugar pucker. For the S sugar pucker (often C2′-*endo*) $^3J_{1'-2'} \cong 10$ Hz, while for N puckers (often C3′-*endo*) $^3J_{1'-2'} \cong$ 1–2 Hz (see Table 2). In 11 nucleotides of the 24-mer, the 2Q{H1′,H2′} pattern could be observed clearly in the 3D spectrum. Most of these are positioned in the loop or bulge region where the furanose conformations have a significant percentage of an S-puckered state. For the 2Q{H1′,H2′} patterns we often found outer intranucleotide NOEs to other

Table 1. Corrected ^{1}H chemical shifts[a] of the RNA 24-mer hairpin at pH 7 and 298 K

Residue	H8/H6	H5/H2	H1′	H2′	H3′	H4′	H5′H5″	
G1	7.63		5.96	4.81	4.88	4.47	*4.58*[b]	*4.27*[b]
G2	8.02		5.90	*4.87*	*4.93*	4.58	*4.47*[b]	*4.38*[b]
G3	8.12		*5.90*	*4.87*	*4.87*	*4.58*	*4.43*[b]	4.27[b]
A4	7.84	7.82	6.00	4.64	*4.50*	*4.59*	4.58[b]	4.13[b]
C5	7.41	5.26	5.37	4.32	4.31	4.42	4.49[b]	4.05[b]
–	–	–	–	–	–	–	–	–
U20	7.70	4.99	5.55	4.47	4.43	4.40	4.53[b]	4.05[b]
C21	7.75	5.55	5.61	4.59	*4.32*	*4.42*	4.49	4.08
U22	7.68	5.60	5.46	4.33	4.40	4.41	4.42	4.07
A23	8.15	7.61	5.82	4.57	4.60	4.22	4.40[b]	4.05[b]
U24	7.50	5.25	5.63	4.07	4.15	4.59	4.28	4.03

[a]Measured at 25 °C; chemical shifts (in ppm, rounded to two decimal spaces) referenced to DSS (4,4-dimethyl-4-silapentane-1-sulfonate; 0.00 ppm) with accuracy of ±0.005 ppm, except for H5′ and H5″ and some overlapping peaks with accuracy of ±0.02. Assignments for **underlined** entries are changed from Borer et al. (1995).
[b]Not stereospecifically assigned; these chemical shift values can be inverted.

sugar protons and base protons, which for the C and U residues could be matched to 2Q{H6,H5} outer NOEs, leading to further assignments. In the 2D-NOE spectrum, overlap in the H1′, H5 region sometimes obscures NOE connectivities to H1′ or H5. For example, U20,1′ and C21,5 resonate at the same frequency. In the 3D NOE/2QC spectrum, however, they show up in different 2Q planes and thus without overlap.

Assignments of the other sugar protons

In the crowded region where the sugar protons H2′ through H5″ resonate (5.0–3.8 ppm), 53 patterns similar to that in Figure 4a could be recognized; Figure 4b shows several of these. An important feature is that $^2J_{5'-5''} \cong 10$ Hz regardless of the sugar pucker. As a consequence, 12 out of 24 2Q{H5′,H5″} patterns were easily picked. Matching the (H5′ and) H5″ outer NOE(s) from the 2Q{H6,H5} or 2Q{H1′,H2′} with those obtained from the strong 2Q{H5′,H5″} led to most of the H5′ and H5″ assignments of the C and U nucleotides; the 2Q{H5′,H5″} often show an outer NOE to the H6 which confirms the H5′ and H5″ assignments. Further corroboration of the H5′ and H5″ assignment was obtained from a ^{31}P-^{1}H COSY spectrum (I. P., and S. Cai P. B., unpublished).

$^3J_{3'-4'}$ and $^3J_{1'-2'}$ values change in an opposite order with sugar pucker (see Table 2). Thus, when the 2Q{H5′,H5″} show outer NOEs to the H3′ and H4′ resonances, they can often be matched with a 2Q{H3′,H4′}, especially in regions dominated by A-helical character. Another aid comes from the 2Q{H2′,H3′} which are nearly always visible since $^3J_{2'-3'} = 3$–7 Hz regardless of the sugar pucker (see Table 2).

Table 2. Useful ^{1}H-^{1}H couplings for creating 2Q coherences in nucleic acids (J in Hz)

Sugar pucker/J-coupling	N	S
$^3J_{5-6}$	∼8	∼8
$^2J_{5'-5''}$	∼10	∼10
$^3J_{1'-2'}$	∼1	∼10
$^3J_{3'-4'}$	∼8	∼1
$^3J_{2'-3'}$	6–7	3–4

Values from Wüthrich, 1986; Davies, 1978.

Another important feature of the 3D-NOE/2QC spectrum is that all of the spins in a given sugar can sometimes be connected by a 'sugar walk', depending on actual coupling constant values. This sugar walk through the 3D spectrum can be accomplished when several two-, or three-bond coupled spins have $J \cong 4$ Hz or more. For conformations with a mixture of N and S puckers, occurring for the 24-mer residues in the hairpin and the bulge, the walk can be easily observed.

A sugar walk is illustrated nicely in Figure 6 for the F2/F1 planes from residue C13. Figure 6a shows the F2/F1 plane at the F3 of C13,2′, with the lower horizontal dashed line at 2Q{H1′,H2′}, F2 = 10.05 ppm

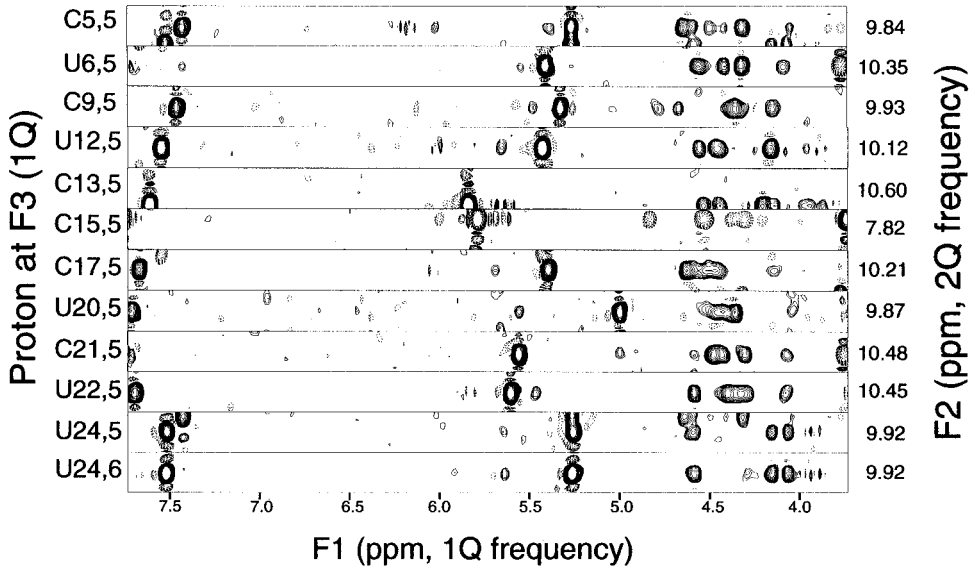

Figure 5. Strips from the 3D NOE/2QC spectrum chosen at the F3 specified, F2 of coupled H5/H6 pairs, with F1 as the horizontal axis; dotted contours outline peaks of opposite sign to solid contours.

serving as a reference. Outer NOE peaks occur for H6, H3′ and H4′ and (weak) H5′/H5″. Since this particular plane is at the C13,2′ frequency in F3, the plane also contains the pattern for the 2Q{H2′,H3′} at the sum of their two chemical shift values (F2 = 8.73 ppm), the upper dashed line in Figure 6a. Because the connectivity patterns for 2Q{H1′,H2′} and 2Q{H2′,H3′} match so well, the H3′ can be assigned securely.

The remainder of the sugar walk occurs in the crowded upfield sugar proton region ($\sim$ 4–5 ppm), so Figure 6b expands the upper-right region from the previous panel. Note that this F2/F1 subplane is still selected at the F3 for C13,2′. There are clear indications of outer NOE contacts to H4′, and to H5′/5″ (with the stronger contact most likely to H5′, see next paragraph). This pattern is repeated in the F2/F1 plane at C13,3′ (not shown). A further match occurs at F2 = 2Q{H3′,H4′}, the lower line in Figure 6c, the subplane selected at F3 = 4.26 ppm (C13,4′). Three outer NOE peaks show up along this line which can be identified as the C13,2′, 5′ and 5″. This pattern is again repeated in the F2/F1 plane at C13,3′ (not shown). Also in panel (c), the upper two lines highlight the 2Q{H4′,H5′} and 2Q{H4′,H5″}. Although these peaks are weak, they further reinforce the H5′ and H5″ assignments. Finally, the H5′ and H5″ assignments are confirmed in panel (d), an F2/F1 subplane selected at the F3 of C13,5′; this pattern repeats at the F3 of C13,5″ (not shown). In panel (d) the H3′ and H4′ occur as clearly defined outer NOE peaks. This discussion emphasizes the extensive redundancy present in the 3D NOE/2QC spectrum that is of considerable aid in verifying assignments.

Tentative stereospecific assignments of the H5′ and H5″ protons can sometimes be made by comparing relative intensities of the H5′ and H5″ peaks in the 2Q{H6,H5} and 2Q{H3′,H4′} patterns. The H3′ – H5′ distance should be significantly shorter for all sugar puckers; this is evident for C13 from the 2Q{H2′,H3′} line in Figure 6b and the 2Q{H3′,H4′} line in Figure 6c. It is also most common for the H5″ to be positioned closer to the base proton than H5′ (data not shown). However, cross peak intensities are a function of both multispin relaxation effects and actual coupling constants, so such assignments are tentative at best.

All of the 185 non-exchangeable proton assignments for the R17 RNA 24-mer were made using the approach just described for interpreting the 3D-NOE/2QC spectrum, along with comparison to deconvolved 2D-NOE subspectra (Borer and Levy, 1994; Borer et al., 1995) matching chemical shifts and fine structure of cross peaks. More information about this combined procedure can be found elsewhere (Borer et al., 1997). In practice, about 80% of the assignments were secured directly from the 3D-NOE/2QC spectrum, with interactive comparison with the 2D-NOE spectrum yielding the remainder. Table 1 corrects

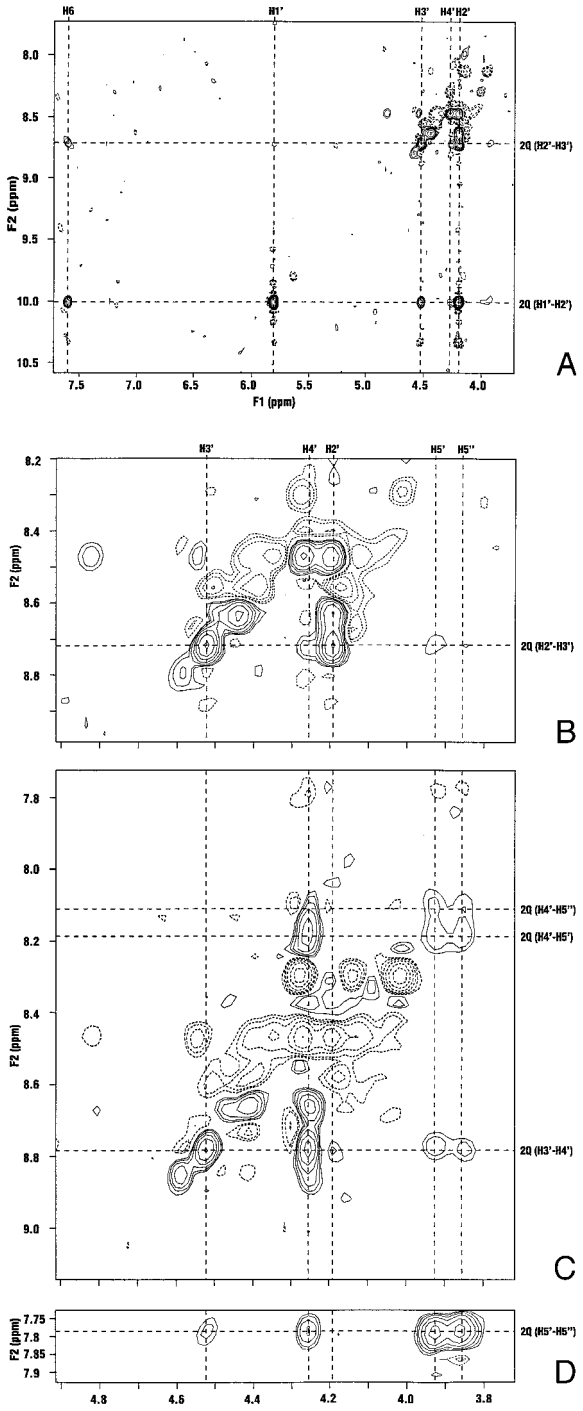

Figure 6. Planes from the 3D-NOE/2QC spectrum illustrating 2Q, as well as inner and outer NOE cross peaks in residue C13. The F1/F2 planes at the H2′ (A,B), H4′ (C) and H5″ (D) of C13 are shown. Dotted lines correspond to negative peaks.

some errors in the previously reported assignment (Borer et al., 1995). Except for the inversion of U20,3′ and 4′, these occur within residues $1-4$, which were especially difficult to assign because of complete overlap of most of the resonances in G2 and G3, and an unusual structure in the strand ends of the molecule that results in many missing NOE correlations. This part of the molecule was not included in the preliminary structure determination reported earlier (Borer et al., 1995). A newly refined structure, based on an average of ∼30 distance restraints per residue from the deconvolved 2D-NOE spectrum, nicely explains the anomaly at the 5′ and 3′ ends of the molecule, and is fully consistent with the present assignment (Kerwood and Borer, 1996). The assignments are also in accordance with the ^{31}P,^{1}H-COSY^{DD} spectrum (I. P., S. Cai, P. B., unpublished).

In summary, it has been shown that for a 24-mer RNA molecule the homonuclear 3D-NOE/2QC spectrum can be very useful in making assignments, with no resort to isotope labeling. It is especially powerful for resonance assignment in crowded regions, such as for the sugar protons in the RNA. This experiment can be useful not only for RNA, but also for DNA where further aid comes from the fact that $^{2}J_{2'-2''} \cong 10$ Hz, even though 2Q{H3′-H4′} are usually lost in a predominantly S-puckered conformation (see Table 2). Other large or highly symmetric biomolecules, such as proteins should also benefit from such applications. 2D ^{1}H-^{13}C correlation experiments at natural abundance (LaPlante et al., 1988; Ashcroft et al., 1989; Varani and Tinoco, 1991), especially the HSQC variant (Bodenhausen and Ruben, 1980), are also useful to classify the *F* region signals into their separate categories in DNA and RNA oligomers. Given the improvements of present-day instrumentation, with field strength as high as 800 MHz, dramatically improved S/N, enhanced multi-axis gradient technology, and ^{31}P-decoupling, we expect that the 3D-NOE/2QC method should apply to even larger and more complex biopolymers.

Acknowledgements

We gratefully acknowledge the assistance and advice of Karl D. Bishop, Sándor Szalma, Anand Vaidyanathan, Mark Roggenbuck, and Christian Griesinger. Useful comments and suggestions from the referees of the manuscript are greatly appreciated. This work was supported in part by grants from the

NIH (GM 32691 to P. B.) and the EXXON Educational Foundation (to I. P.).

References

Ashcroft, J., LaPlante, S.R., Borer, P.N. and Cowburn, D. (1989) *J. Am. Chem. Soc.*, **111**, 363–365.

Batey, R.T., Inada, M., Kujawinski, E., Puglisi, J.D. and Williamson, J.R. (1992) *Nucleic Acids Res.*, **20**, 4515–4523.

Batey, R.T., Battiste, J.L. and Williamson, J.R. (1995) *Methods Enzymol.*, **261**, 300–322.

Bax, A., Freeman, R. and Kempsell, S.P. (1980) *J. Am. Chem. Soc.*, **102**, 4849–4851.

Bax, A., Griffey, R.H. and Hawkins, B.L. (1983) *J. Magn. Reson.*, **55**, 301–315.

Bax, A., Ikura, M., Kay, L.E. and Zhu, G.J. (1991) *J. Magn. Reson.*, **91**, 174–178.

Berthault, P. and Perly, B. (1989) *J. Magn. Reson.*, **81**, 631–634.

Bishop, K.D., Borer, P.N. and Pelczer, I. (1996) *J. Magn. Reson.*, **B110**, 9–15.

Bodenhausen, G. and Ruben, D.J. (1980) *Chem. Phys. Lett.*, **69**, 185–189.

Borer, P.N. and Levy, G.C. (1994) *Methods Enzymol.*, **239**, 257–288.

Borer, P.N., Lin, Y., Wang, S., Roggenbuck, M.W., Gott, J.M., Uhlenbeck, O.C. and Pelczer, I. (1995) *Biochemistry*, **34**, 6488–6503.

Borer, P.N., Pappalardo, L., Kerwood, D.J. and Pelczer, I. (1997) *Adv. Biophys. Chem.*, **6**, 173–216.

Braunschweiler, L., Bodenhausen, G. and Ernst, R.R. (1983) *Mol. Phys.*, **48**, 535–560.

Cieslar, C., Holak, T.A. and Oschkinat, H. (1990) *J. Magn. Reson.*, **87**, 400–407.

Dalvit, C., Wright, P.E. and Rance, M. (1987) *J. Magn. Reson.*, **71**, 539–543.

Davies, D.B. (1978) *Prog. NMR Spectrosc.*, **12**, 135–226.

Davis, D.G. (1989) *J. Magn. Reson.*, **81**, 603–607.

Gott, J.M., Pan, T., LeCuyer, K.A. and Uhlenbeck, O.C. (1993) *Biochemistry*, **32**, 13399–13404.

Griesinger, C., Sørensen, O.W. and Ernst, R.R. (1989) *J. Magn. Reson.*, **84**, 14–63.

Hoult, D.I. and Richards, R.E. (1975) *Proc. R. Soc. London, Ser. A*, **344**, 311–352.

Jahnke, W. and Kessler, H. (1994) *J. Biomol. NMR*, **4**, 735–740.

Jeener, J., Meier, B.H., Bachmann, P. and Ernst, R.R. (1979) *J. Chem. Phys.*, **71**, 4546–4553.

Kerwood, D.J. and Borer, P.N. (1996) *Magn. Reson. Chem.*, **34**, S136–S146.

Kessler, H., Gehrke, M. and Griesinger, C. (1988) *Angew. Chem. Int. Ed. Engl.*, **27**, 490–536.

Kessler, H., Mronga, S. and Gemmecker, G. (1990) *J. Magn. Reson.*, **87**, 633–638.

LaPlante, S.R., Ashcroft, J., Cowburn, D., Levy, G.C. and Borer, P.N. (1988) *J. Biomol. Struct. Dyn.*, **5**, 1089–1099.

Lowary, P.T. and Uhlenbeck, O.C. (1987) *Nucleic Acids Res.*, **15**, 10483–10493.

Macura, S., Kumar, N.G. and Brown, L.R. (1984) *J. Magn. Reson.*, **60**, 99–105.

Mareci, T.H. and Freeman, R. (1983) *J. Magn. Reson.*, **51**, 531–535.

Mareci, T.H. (1988) In *Pulse Methods in 1D and 2D Liquid-Phase NMR* (Ed., Brey, W.S.), Academic Press, New York, NY, pp. 259–341.

Marion, D., Ikura, M. and Bax, A. (1989) *J. Magn. Reson.*, **84**, 425–430.

Michnicka, M.J., Harper, J.W. and King, G.C. (1993) *Biochemistry*, **32**, 395–400.

Mooren, M.M.W., Hilbers, C.W., van der Marel, G.A., van Boom, J.H. and Wijmenga, S.S. (1991) *J. Magn. Reson.*, **94**, 101–111.

Morris, G.A. and Freeman, R. (1987) *J. Magn. Reson.*, **29**, 433–462.

Müller, L. and Pardi, A. (1985) *J. Am. Chem. Soc.*, **107**, 3484–3487.

Neuhaus, D. and Williamson, M.P. (1989) *The Nuclear Overhauser Effect in Structural and Conformational Analysis*, VCH Publishers, Inc., New York, NY, pp. 284–285.

Nikonowicz, E.P., Sirr, A., Legault, P., Jucker, F.M., Baer, L.M. and Pardi, A. (1992) *Nucleic Acids Res.*, **20**, 4507–4513.

Oschkinat, H., Cieslar, C., Holak, T.A., Clore, G.M. and Gronenborn, A.M. (1989) *J. Magn. Reson.*, **83**, 450–472.

Oschkinat, H., Cieslar, C. and Griesinger, C. (1990) *J. Magn. Reson.*, **86**, 453–469.

Otting, G. (1990) *J. Magn. Reson.*, **86**, 496–508.

Pelczer, I. and Szalma, S. (1991a) *Chem. Rev.*, **91**, 1507–1524.

Pelczer, I., Bishop, K.D., Levy, G.C. and Borer, P.N. (1991b) *J. Magn. Reson.*, **91**, 604–606.

Pelczer, I., Hoch, J.C., Roggenbuck, M.W., Vaidyanathan, A., Leccarde, M.G. and Borer, P.N. (1992) In *NMRZ User Guide*, Tripos Assoc., St. Louis, MO.

Pelczer, I. and Bishop K.D. (1997) In *Methods for Structure Elucidation by High-Resolution NMR* (Eds. Kövér, K.E., Batta, Gy. and Szántay Jr., Cs.), Elsevier, New York, NY, pp. 187–207.

Pelczer, I. and Carter, B.G. (1997) In: *Protein NMR Techniques*, Vol 60. in the Series: *Methods in Molecular Biology* (Ed., Reid, D.G.), Humana Press, Totowa, NJ, pp. 71–156.

Piotto, M.E. and Gorenstein, D.G. (1991) *J. Am. Chem. Soc.*, **113**, 1438–1440.

Piotto, M., Saudek, V. and Sklenár, V. (1992) *J. Biomol. NMR*, **2**, 661–665.

Radhakrishnan, I., Patel, D.J. and Gao, X. (1992) *Biochemistry*, **31**, 2514–2523.

Rance, M. and Byrd, A. (1983) *J. Magn. Reson.*, **52**, 221–240.

Romaniuk, P.J., Lowary, P., Wu, H.-N., Stormo, G. and Uhlenbeck, O.C. (1987) *Biochemistry*, **26**, 1563–1568.

Simorre, J.-P. and Marion, D. (1991) *J. Magn. Reson.*, **94**, 426–432.

Simorre, J.-P., Caille, A., Marion, D. and Ptak, M. (1991) *Biochemistry*, **30**, 11600–11608.

Sklenár, V. (1995) *J. Magn. Reson.*, **A114**, 132–135.

States, D.J., Haberkorn, R.A. and Ruben, D.J. (1982) *J. Magn. Reson.*, **48**, 286–292.

Stejskal, E.O. and Schaefer, J. (1974) *J. Magn. Reson.*, **14**, 160–169.

van de Ven, F.J.M., Haasnoot, C.A.G. and Hilbers, C.W. (1985) *J. Magn. Reson.*, **61,** 181–187.

Varani, G. and Tinoco Jr., I. (1991) *J. Am. Chem. Soc.*, **113**, 9349–9354.

Vuister, G.W., Boelens, R. and Kaptein, R. (1988) *J. Magn. Reson.*, **80**, 176–185.

Wang, K.-Y. (1991) Ph. D. Thesis, Syracuse University.

Wijmenga, S.S., Heus, H.A., Werten, B., van der Marel, G.A., van Boom, J.H. and Hilbers, C.W. (1994) *J. Magn. Reson.*, **B103**, 134–141.

Williamson, M.P. and Neuhaus, D. (1987) *J. Magn. Reson.*, **72**, 369–375.

Wu, N.-H. and Uhlenbeck, O.C. (1987) *Biochemistry*, **26**, 8221–8227.

Wüthrich, K. (1986) *NMR of Proteins and Nucleic Acids*, Wiley, New York, NY.

Zuiderweg, E.R.P., Hallenga, K. and Olejniczak, E.T. (1986) *J. Magn. Reson.*, **70**, 336–343.